JCIM JOURNAL OF CHEMICAL INFORMATION AND MODELING

pubs.acs.org/jcim

Article

Flexibility and Hydration of the Q_o Site Determine Multiple Pathways for Proton Transfer in Cytochrome bc_1

Published as part of Journal of Chemical Information and Modeling special issue "Computational Chemistry in the Global South: The Latin American Perspective."

Sofia R. G. Camilo and Guilherme M. Arantes*

Cite This: J. Chem. Inf. Model. 2025, 65, 6184−6197

Read Online

ACCESS | Metrics & More | Article Recommendations | Supporting Information

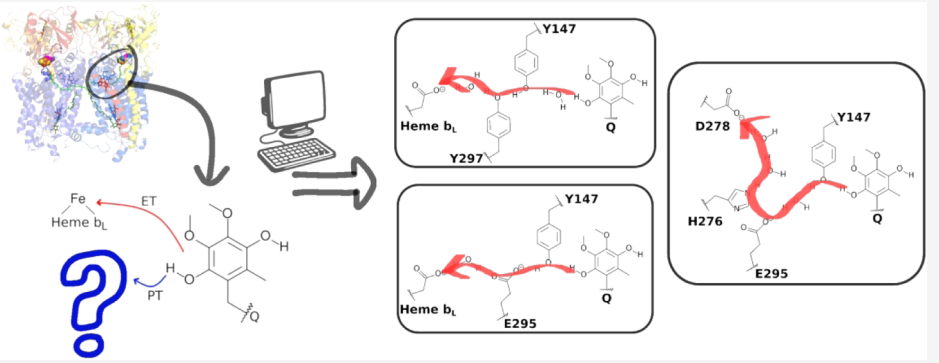

ABSTRACT: The detailed catalytic activity of cytochrome bc_1 (or respiratory complex III) and the molecular mechanism of the Q cycle remain elusive. At the Q_o site, the cycle begins with oxidation of the coenzyme-Q substrate (quinol form) in a bifurcated two-electron transfer to the iron−sulfur (FeS) cluster and the heme b_L center. The release of two protons during quinol oxidation and their transfer is less understood, with one proton likely delivered to the histidine side chain attached to the FeS cluster. Here, we present extensive molecular dynamics simulations with enhanced sampling of side-chain torsions at the Q_o site and analyze available sequences and structures of several bc_1 homologs to probe the interactions of quinol with potential proton acceptors and identify viable pathways for proton transfer. Our findings reveal that side chains at the Q_o site are highly flexible and can adopt multiple conformations. Consequently, the quinol head is also flexible, adopting three distinct binding modes. Two of these modes are proximal to the heme b_L and represent reactive conformations capable of electron and proton transfer, while the third, more distal mode likely, represents a prereactive state, consistent with recent cryo-EM structures of bc_1 with bound coenzyme-Q. The Q_o site is highly hydrated, with several water molecules bridging interactions between the quinol head and the conserved side chains Tyr147, Glu295, and Tyr297 in cytochrome *b* (numbering according to *Rhodobacter sphaeroides*), facilitating proton transfer. A hydrogen bond network and at least five distinct proton wires are established and possibly transport protons via a Grotthuss mechanism. Asp278 and propionate-A of heme b_L in cytochrome *b* are in direct contact with external water and are proposed as the final proton acceptors. The intervening water molecules in these proton wires exhibit low mobility, and some have been resolved in recent experimental structures. These results help to elucidate the intricate molecular mechanism of the Q-cycle and pave the way to a detailed understanding of chemical proton transport in several bioenergetic enzymes that catalyze coenzyme-Q redox reactions.

INTRODUCTION

Cytochrome bc_1 and its homolog cytochrome b_6f are essential proteins respectively for cellular respiration and photosynthesis. As part of electron transport chains, these enzymes balance the redox state of coenzyme-Q (quinol/quinone forms, here abbreviated by Q) in the membrane pool and contribute to the transmembrane electrochemical potential via the Q-cycle reaction.[1−4] Cytochrome bc_1 is a major producer of reactive oxygen species[5] and is involved in various metabolic disfunctions.[6] Inhibitors of the bc_1 activity have wide biomedical and biotechnological relevance for controlling pathogens, such as in treatment of pneumonia and malaria[7] and as commercial fungicides used in agriculture.[8]

Received: March 25, 2025
Revised: May 12, 2025
Accepted: June 3, 2025
Published: June 10, 2025

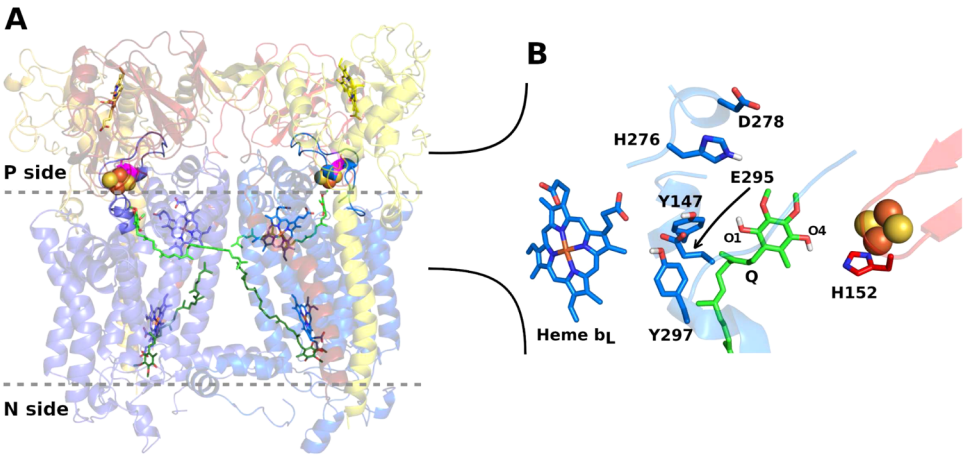

Figure 1. Structure of the cytochrome bc_1 dimer complex of *R. sphaeroides* (PDB ID 2qjp).[9] (A) Essential catalytic units in the bc_1 dimer in cartoon with cytochrome *b* (cyt *b*) in blue, cytochrome c_1 in yellow, and Rieske protein in red. Membrane interface is in gray dashes with Q molecules in green sticks and modeled in quinol form bound to the Q_o site (membrane P side) and quinone form bound to the Q_i site (N side). FeS clusters are in orange and yellow spheres, hemes b_L (near site Q_o) and b_H (near site Q_i) in blue sticks, hemes *c* in yellow and cyt *b* D278 in magenta. (B) Close view in a rotated angle of the Q_o site with labels in residues and in phenolic oxygens of the Q substrate, which was manually modeled by replacing the inhibitor stigmatellin.

The structure of cytochrome bc_1 is a dimer (Figure 1) and each monomer has three essential subunits: cytochrome *b* (cyt *b*), cytochrome c_1 and the Rieske protein, complemented by (up to 8) organism-specific supernumerary units. Each monomer has two distinct active sites, Q_o and Q_i, where two-electron oxidation and reduction of Q substrates occur. Two *b*-type hemes in cyt *b*, hemes b_L and b_H labeled after their relative Low and High redox potentials, mediate electron transfer from the Q_o site to the Q_i site. A *c*-type heme in cytochrome c_1 mediates electron transfer from a [2Fe-2S] cluster, also part of the Q_o site, to the soluble cytochrome *c*. This FeS cluster is bound to the Rieske protein by two histidine residues (His131 and His152 in *R. sphaeroides* numbering) and two cysteines (Cys129 and Cys149).[3,10]

Despite its importance, the molecular mechanism of the Q-cycle catalyzed by cytochrome bc_1 is still not completely elucidated.[4,11] In the Q_o site, the two-electron oxidation of the Q substrate in quinol form (dihydroquinone) is a bifurcated process,[12] with one electron transferred to the FeS cluster with high redox potential and another electron transferred to heme b_L. In concert, two chemical protons are released from Q (resulting in the quinone form) and translocated to the membrane P side (Figure 1). An important open question about the Q-cycle concerns the identity and the structure of protein groups in the Q_o site involved in the release and transport of these chemical protons.

Experimental structures with atomic resolution containing a Q molecule bound to the complete Q_o site were observed only recently by cryo-EM microscopy.[13−19] The Q substrate occupies a position similar to that previously determined for the inhibitor stigmatellin (Figure 1B).[4,9] The phenolic oxygen O_4 in the Q-head (Q_{O_4}) and the side chain of H152 in the Rieske protein clearly interact and hydrogen-bond (H-bond) in some models.[15−18] These observations confirm previous proposals about the essential role of H152 in substrate binding[4] and as the acceptor of one chemical proton.[2,20] Direct titration of the H152 side chain in NMR experiments under different redox conditions,[21] and various computer simulations of molecular dynamics (MD) in the Q_o site[22−26] and of the proton-coupled electron transfer reaction between quinol and H152[26,27] also support that this residue is one of the proton acceptors.

The binding interactions and groups involved in proton transfer from the other Q phenolic oxygen (O1) in the Q_o site are not clearly established. Single-point mutations in Y147[28] and E295[4,29] in cyt *b* (Figure 1B) suggested these residues are important for Q binding and proton release. MD simulations have shown that Q_{O1} in quinol form may H-bond with side chains of Y147 and E295,[23] and with water molecules.[22] However, cryo-EM structures do not confirm direct interactions with these residues, which are distant by at least 0.8−1.0 nm from Q_{O1} in all Q bound models.[15−18] Based on recent mutational studies, His276 and Asp278 in cyt *b* were also proposed as possible acceptors of this secondary chemical proton.[30]

Proton transport within proteins occurs through proton-wires, which are series of connected molecules that transfer an excess H^+ from the initial donor to the bulk solvent. Water molecules and protonable groups, such as acidic side chains, are the most common components.[31−33] A notable example is proton transport in cytochrome *c* oxidase (CcO or respiratory complex IV), where proton-wires composed of various side chains and propionate groups of redox-active heme centers have been proposed.[34−36] Proton conduction is achieved through the Grotthuss mechanism, which involves the breaking and forming of covalent hydrogen bonds and the reorientation of participating groups. Therefore, the composition, structure, and conformational flexibility of the participants in a proton-wire, along with their electrostatic interactions with the surrounding environment, are crucial to wire stability and transport efficiency. These properties have often been studied using molecular simulations.[37]

Here, we seek the molecular groups involved in the transport of chemical protons released by the quinol substrate in the Q_o site of cytochrome bc_1. We first analyze multiple sequences of cytochrome *b* to find conserved residues spatially near the Q_o site that could act as proton acceptors. Considering the residues previously mentioned, we identify that cyt *b* Y147, E295, and Y297 are highly conserved, but H276 and D278 are not. To probe the conformational landscape and detailed interactions

https://doi.org/10.1021/acs.jcim.5c00655
J. Chem. Inf. Model. 2025, 65, 6184−6197

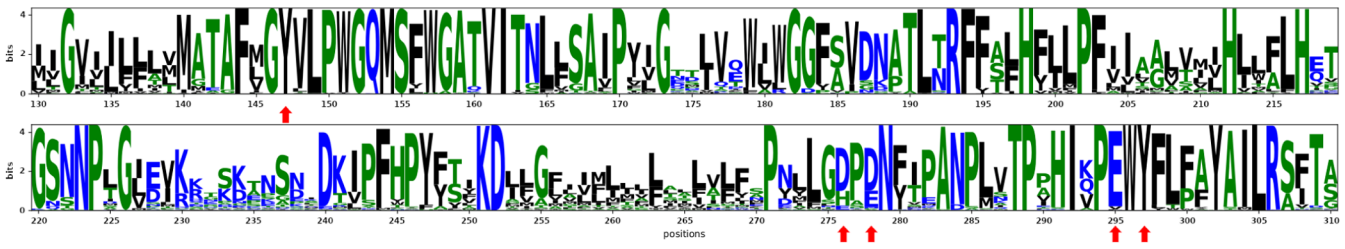

Figure 2. Residue conservation for cytochrome *b* shown as a WebLogo.[42] Red arrows point to residue positions studied in the following sections (Y147, E295, Y297, H276, and D278).

among these residues and the quinol substrate, we conducted molecular dynamics simulations one order of magnitude longer than previously reported[22,23,25] employing a force-field calibrated for Q interactions that provides superior performance.[38,39] We also employed metadynamics[40] simulations to increase sampling of Y147, E295, and Y297 side chain torsions. These methodological enhancements led to high quality models of the molecular flexibility of side chains and the Q-head, and of internal hydration describing a network of H-bonds in the Q_o site, in agreement with the collection of experimental structures available. We identify Y147 as the initial proton acceptor from Q_{O1} and propose, for the first time, that the heme b_L propionate-A (PRA_{b_L}) is the final acceptor of the secondary proton, before releasing it to bulk water. We describe molecular wires[33] that may transport the chemical protons released from oxidized Q via a Grotthuss mechanism[32] and conclude that residues used by cytochrome bc_1 to transport protons may be used similarly in other respiratory enzymes that catalyze Q redox reactions.

METHODS

Multiple Sequence Alignment. Starting from the protein sequence of *R. sphaeroides* cytochrome *b* (Uniprot Q02761), a multiple sequence alignment from the region surrounding the Q_o site (residues 130 to 310) was performed using the MPI Bioinformatics Toolkit[41] against the Uniref90_30_jun database. This was used to determine consensus residues that could participate in catalysis by the Q_o site. All parameters were kept as default except it max target hits which was set to 10,000. Sequences containing more than 25% gaps were removed. WebLogo was used to generate the sequence conservation plot in Figure 2.[42]

Analysis of Experimental Structures. The conformational distribution of side chains in the Q_o site was analyzed by collecting 52 entries deposited in the Protein Data Bank (PDB), comprising 47 structures from cytochrome bc_1 (35 from bc_1 alone, 7 from supercomplex SC III–IV and 5 from SC I–III) and 5 from cytochrome b_6f (homologous to bc_1). A total of 30 models were obtained through X-ray crystallography and 22 were obtained through cryo-EM; 17 PDB entries had structural waters built into the model, and 13 entries had a Q substrate bound in the Q_o site. Only one bc_1 monomer was present in some of the structures, so we analyzed a total of 79 models of the Q_o site. More details of all PDB entries and their references are listed in the Supporting Information (SI).

Set-up of Molecular Models. A model of the cytochrome bc_1 protein complex was constructed based on the X-ray crystal structure of *R. sphaeroides* (PDB 2qjp[9]). This model lacks subunit IV, which was recently revealed (PDB 8asi[15]) to be placed at the opposite side of the bc_1 complex, more than 30 Å away from the Q_o site. Thus, the lack of subunit IV in our model should not interfere with any of our simulation results and conclusions. It should also be noted that *R. capsulatus* contains a fully active cytochrome bc_1 which monomer is formed only by the three essential subunits.[4] Inhibitors and detergent molecules were removed, while six tetra-linoleoyl cardiolipins were added, following their positions from a superimposed yeast model (PDB 1kb9[43]). Crystallographic waters were preserved and additional molecules were inserted in line with internal hydration observed in more recent bc_1 structures.[15−17] Ubiquinone-6 (Q_6, with 6 isoprenoid units) was modeled in both Q_i sites of the dimer. The oxidized form of Q_6 was used, and its positions were adjusted through manual docking in PyMOL,[44] with the Q-head replacing the antimycin inhibitor and isoprenoid units arranged in a U-shaped conformation. In both Q_o sites, Q_6 was modeled in the reduced quinol (QH_2) form, N_ϵ in H152 in Rieske protein was deprotonated, and the [2Fe-2S] cluster was oxidized. The Q molecule was manually placed, and its head replaced stigmatellin, with isoprenoid units arranged in an extended conformation. The protonation states of side chains were adjusted to positive charge in K and R residues, negative in D and E residues, and all other residues were treated as neutral, except for Asp373, exposed to the membrane in subunits cyt *b*, which was protonated. His tautomers and missing side chain atoms were assigned using WhatIf.[45] H131 in Rieske protein, which also binds the FeS cluster, was modeled with a protonated N_ϵ.[21] The protein complex was embedded in a solvated POPC (1-palmitoyl-2-oleoyl-*sn*-glycero-3-phosphocholine) membrane with 512 lipid molecules, 39,102 water molecules, 214 Na^+ and 158 Cl^- ions. These ions maintain a neutral total system charge and a salt concentration of approximately 0.1 M. The complete solvated model comprised 215,264 atoms.

Classical Molecular Dynamics Simulations. Interactions between proteins, lipids, and ions were described using the all-atom CHARMM36m force-field,[46−48] while standard TIP3P[49] was used to represent water molecules. Q was described using our calibrated force-field,[38,39] and FeS clusters were represented using the Chang and Kim[50] parameters, with calibrated charges for Cys and His side chain ligands given in Table S2. Oxidized heme groups were described using parameters by Luthey–Schulten et al.,[51] with vinyl side chains in heme *b* replacing the thioether linkages of heme *c* (Table S2).

After initial geometry optimization with a conjugated-gradient minimizer, four molecular dynamics (MD) simulations of 50 ns each were performed to relax and equilibrate the complete solvated model. Harmonic restraints were applied to tether protein heavy atoms to their initial positions in the first simulation, and these restraints were successively diminished in subsequent runs, ultimately reaching zero in the final simulation. MD simulations were carried out with constant temperature (310 K) and pressure (1 atm), and a time step of 2 fs. Long-range electrostatics were treated with the Particle Mesh Ewald

https://doi.org/10.1021/acs.jcim.5c00655
J. Chem. Inf. Model. 2025, 65, 6184−6197

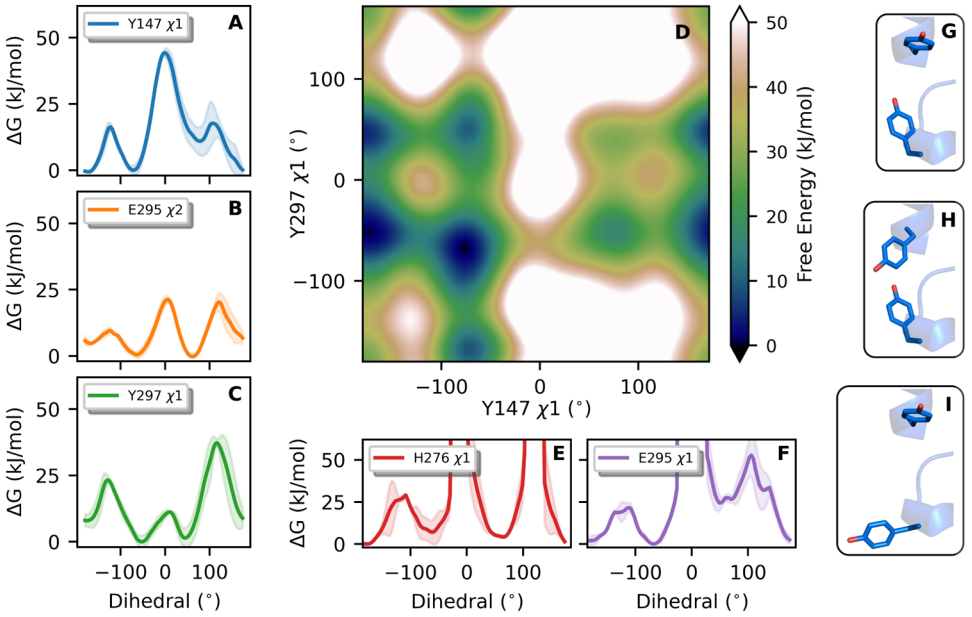

Figure 3. Conformational landscape of residues in the Q_o site depicted as free energy surfaces (ΔG). Side-chain torsions in cyt *b* residues indicated in the legend are shown in (A–F), with a 2D-profile shown in (D) for $\chi 1$ in both Y147 and Y297. 1D-profiles show the average of two independent metadynamics simulations, with colored shadows representing the standard error. Torsions of dihedrals $\chi 1$ in Y147 and Y297, and $\chi 2$ in E295 (A–C) were boosted in the metadynamics, while torsions of $\chi 1$ in H276 and in E295 were not. Thus, discontinuities in (E, F) represent undersampled regions. Illustrative structures for (Y147, Y297) side chains are shown respectively for conformers (*t*, *g*) in (G), (−*g*, *g*) in (H) and (*t*, −*g*) in (I).

method.[52] Visualization and figure plotting were performed using PyMOL[44] and Matplotlib.[53] A productive canonical MD trajectory was obtained with a total time of 550 ns using GROMACS version 2016.3.[54]

Starting from a snapshot at 400 ns of this trajectory, two additional simulations lasting 795 ns each were produced with metadynamics to enhance sampling of flexible residues in the Q_o site. In one simulation, well-tempered metadynamics[40] was activated simultaneously in the torsion of dihedrals $\chi 1$ of Y147 and Y297, and $\chi 2$ of E295 of cytochrome *b* in one monomer (chain A). The second simulation had metadynamics activated simultaneously in the same dihedrals but for the other monomer (chain D). Gaussians were deposited every 1000 time steps (2 ps), at initial height of 0.6 kJ mol^{-1}, widths of 0.4 and a bias factor of 15. Metadynamics was run with GROMACS version 2020.2 and the PLUMED plugin version 2.6.1.[55]

Two types of analysis were performed in the simulations. Free energy analysis is preferred because it accounts for population differences and for statistical significance of simulated processes and interactions.[56] However, meaningful free energy profiles require extensive sampling and thus, were only used here for torsions and pair distances directly involving residues Y147, E295, and Y297. Conformational sampling for these side chains was enhanced by metadynamics, so it is expected that their torsion profiles will be the most precise (as confirmed by smaller standard errors observed in Figure 3A–C). Sampling of pair distances was not directly enhanced so free energy profiles for distances will have lower precision. In all free energy profiles, the metadynamics bias was removed by reweighting the distributions. Interactions involving other groups and water solvation were analyzed by trajectories of atom-pair distances and of water bridge contacts, which were considered to be formed when both distances from the bridge water oxygen to the H-bond donor and acceptor are simultaneously smaller than 0.35 nm. The six trajectories shown for each property analyzed in the Results and Discussion section represent local sampling starting from different initial conformations and thus, will naturally show different histogram distributions (Count) due to the finite and localized sampling. The dispersion between these distributions is expected to be higher and the analysis of the respective property should be only qualitative.

RESULTS AND DISCUSSION

Y147, E295, and Y297 in cyt *b* are Highly Conserved while H276 and D278 are Not. Protein residues with high conservation along the evolutionary process are expected to have important structural and catalytic roles. We employed a multiple sequence alignment (MSA) to explore residue conservation in cytochrome *b* (9993 sequences with $1.36 \times 10^{-123} < e\text{-value} < 2.00 \times 10^{-51}$ from the *R. sphaeroides* sequence) and found that most of the residues in the Q_o site are highly conserved, as shown graphically in Figure 2. Focusing in side chains that may change protonation state and participate in proton transport near the Q binding site, residues Y147, E295 and Y297 (here named as YEY group) show 99.9, 94.2, and 98.9% conservation, respectively, raising to 100, 99.7, and 100% among 329 sequences curated in the Swiss-Prot database as active enzymatic subunits.[57] For comparison, residues Pro294 and Trp296, in the often studied and conserved PEWY motif,[58−61] are conserved in 99.3 and 99.0% sequences in the full set. No double mutations among the YEY residues were observed, which could indicate a coevolutionary dependence.

H276 and D278 have much lower conservation, 23.4 and 68.3% in the full set, and 10.2 and 80.1% for the sequences in Swiss-Prot, suggesting that these are not essential residues for function. These positions are often substituted by acidic residues (H276D and D278E) which may also transport protons, particularly in ϵ−proteobacteria, which commonly inhabit acidic environments.[61,62] Additionally, a notable portion of sequences (~1.2%) have substitutions at position 276 with residues incapable of proton conduction. Therefore, a more

https://doi.org/10.1021/acs.jcim.5c00655
J. Chem. Inf. Model. 2025, 65, 6184−6197

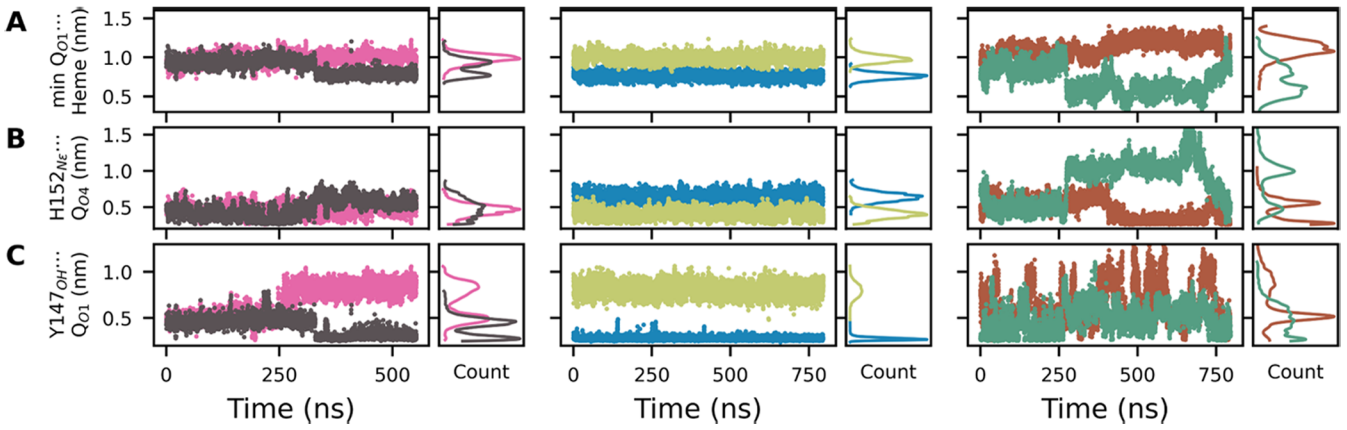

Figure 4. Atom-pair distances involving the substrate Q-head in the Q_o site during simulations. Pairs are given in *Y*-axis labels. Left and middle columns show canonical MD simulations, right column shows metadynamics simulations. Each column shows two trajectories corresponding to the two Q_o sites of the bc_1 dimer. Count shows a histogram of the respective distance.

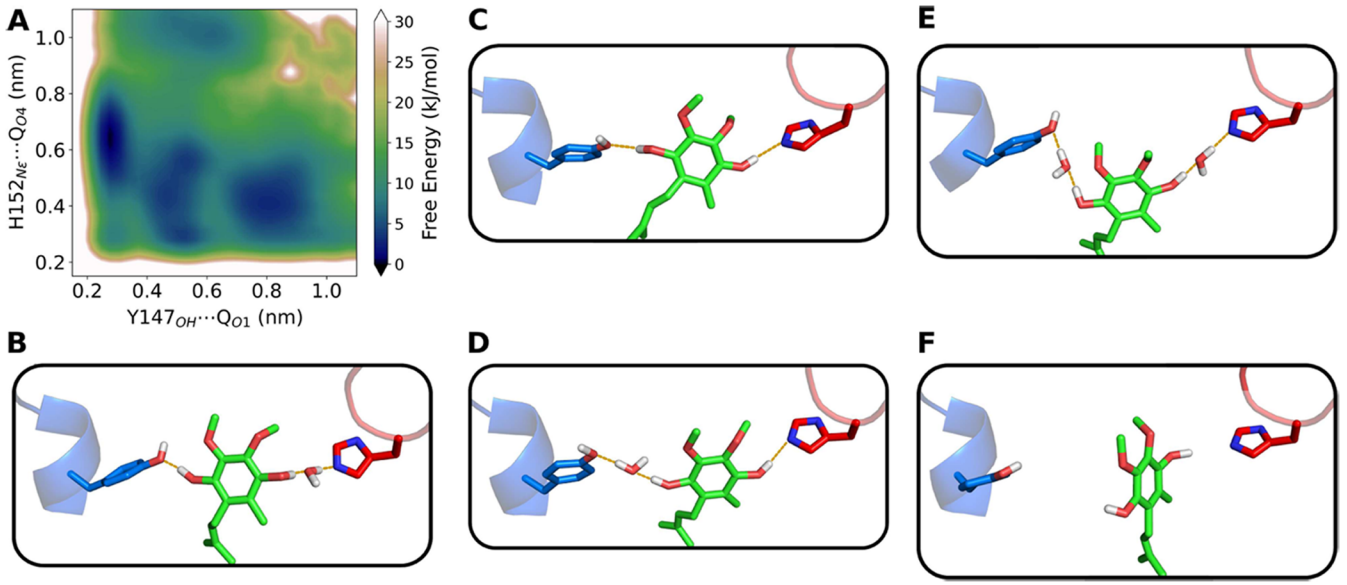

Figure 5. Conformational landscape of the substrate Q-head bound in the Q_o site. (A) Free energy surface in relation to distances between Q substrate phenolic oxygens and Q_o site residues. Representative snapshots of Y147 (blue), H152 (red) and the Q-head (green) conformations with H-bonds displayed as orange dashes are shown for distance pairs ($Y147_{OH}$···Q_{O_1}, $H152_{N_\varepsilon}$···Q_{O_4}) in nm: (B) (0.3,0.6), (C) (0.3,0.3), (D) (0.5,0.3), (E) (0.5,0.5) and (F) (0.8,0.4). The Y147 side-chain is shown in the *t* form for all snapshots, but its −*g* conformer may also establish H-bonds similar to those in (B, D, E) models.

detailed analysis is required to clarify the roles of H276 and D278 in the Q_o site.

Although we focused on high similarity (low *e*-values were used to determine our MSA), our conclusions on residue conservation are comparable to those obtained by Hunte et al., who used a more diverse and less similar sequence set focused on the PEWY motif.[61] Their study suggests parallel evolution of the Q_o site at position 295, occupied by glutamate when the substrate is ubiquinone and aspartate when the substrate is menaquinone, with lower redox potential. In position 297, only mutations from Tyr to Phe were observed in their sequence set. The respective organisms always possess extra cyt *b* sequences, suggested to perform different function such as thiosulfate oxidation.[61]

MD Simulations Unveil the Flexibility of Conserved Residues and of the Substrate Q-Head in the Q_o Site. The conformational landscape and intermolecular contacts of the Q_o site bound with the Q substrate were explored by three long molecular dynamics simulations modeling the reactant Michaelis complex of cytochrome bc_1. The expected charge state before electron and proton transfers was assigned as the Q substrate in quinol form (doubly reduced and doubly protonated) with heme b_L and the [2Fe-2S] cluster in oxidized form. The H152 side chain was bound to the FeS cluster (via N_δ) and deprotonated (at N_ϵ). Two simulations of 795 ns had metadynamics activated to enhance sampling of torsion angles $\chi 1$ of Y147, $\chi 2$ of E295, and $\chi 1$ of Y297 in a single Q_o site. Because cytochrome bc_1 is a dimer, two canonical MD trajectories of the same length (795 ns) for the other monomer not activated by metadynamics, were also produced. These add to the initial MD simulations of 550 ns, giving a total of four canonical MD trajectories of the Q_o site (2×550 ns + 2×795 ns). All simulations were stable and maintained the global fold

https://doi.org/10.1021/acs.jcim.5c00655
J. Chem. Inf. Model. 2025, 65, 6184−6197

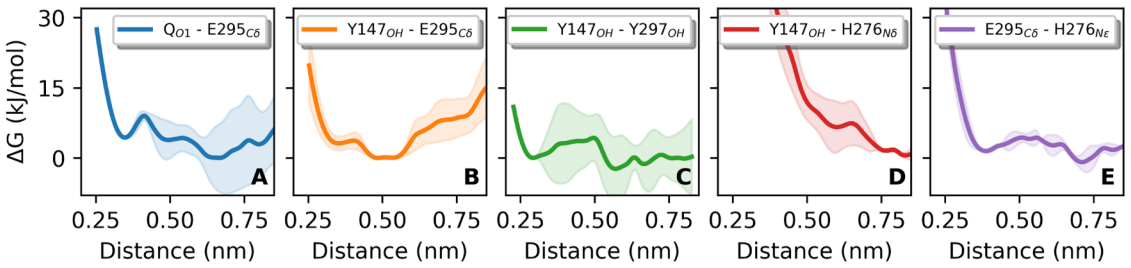

Figure 6. Stability of direct interactions in the Q_o site depicted as free energy (ΔG) profiles for the contacts indicated in the legend of each panel. Lines show the average of two independent metadynamics simulations and colored shadows represent the standard error.

and backbone configuration of protein subunits, even when metadynamics was activated (Figures S1 and S2 in SI).

Side-chains in the YEY group and H276 populate *t* (χ angle ~ 180°, defined using the quartet N−Cα-Cβ-Cγ), *g* (60°), and −*g* (−60°) conformers, indicating high flexibility in the Q_o site, as shown in the obtained torsion profiles (Figure 3). For Y147 and Y297, five pairs of conformers may be populated (blue regions in Figure 3D), with the most likely pairs being (*t*, −*g*) and (*t*, *g*), illustrated in Figure 3G,I. Barriers for transitions between these populated conformers, such as from $-g \rightarrow t$ of the Y147 side chain, are between 10 and 25 kJ/mol. Thus, interconversions occur on the ns-time scale and should not gate proton and electron transfers for the initial reactant state simulated here.

As discussed in the section, "Experimental Structures Confirm that Qo Side Chains are Flexible and Highly Hydrated" analysis of tens of bc_1 structures deposited in the PDB confirms that the multiple conformations of the YEY group side chains obtained here are also experimentally observed.

Interactions of the bound substrate Q-head in the Q_o site were identified through distance trajectories taken from MD simulations. Figure 4A shows the minimum distance between the quinol phenolic oxygen O_1 and heme b_L is always under 1.5 nm. Thus, conformations probed in simulations are capable of fast electron transfer between the Q substrate and heme b_L. In Figure 4B, the distance between O_4 and H152 N_ϵ is consistently lower than 0.6 nm, except in one metadynamics trajectory (colored green) between 250 to 680 ns, when the Q-head bends toward heme b_L and O_4 moves away from H152. A direct H-bond is established between O_4 and H152 N_ϵ when their distance is 0.35 nm, and a bridged interaction by one water molecule is established when their distance is 0.5−0.6 nm (a detailed description of local solvation and water-bridge contacts is given below in the section "Q_o Site is Highly Hydrated and Has Several Water-Bridged Connections between Side ChainsChains"). A similar observation is made from Figure 4C, where three characteristic distances between quinol Q_{O_1} and Y147$_{OH}$ are observed, corresponding to the three peaks at 0.3, 0.5, and 0.9 nm in Count distributions. A direct H-bond and a one-water bridge interaction are observed for distances of 0.3 and 0.5 nm, respectively (Figure 5B−E).

Multiple minima for the interaction of the Q-head with Y147 and H152 side chains in the Q_o site are revealed in the free energy profile shown in Figure 5A, suggesting that the bound Q substrate is also highly flexible. This profile was obtained by combining the six trajectories of Figure 4B−C, with an aggregate time of 4.3 μs of MD simulation.

Three binding modes were identified with similar stability, corresponding to free energy minima (dark blue regions in Figure 5A) found at Y147$_{OH}$···Q_{O_1} distances of 0.3, 0.5, and 0.85 nm. The first mode (at 0.3 nm, "proximal" to heme b_L) is the most stable and is separated from other minima by interconversion barriers of 10 to 20 kJ/mol. It is characterized by a direct H-bond between Q_{O_1} and Y147$_{OH}$ and a water-bridged interaction between Q_{O_4} and H152$_{N_\epsilon}$ (Figure 5B). The second mode (at 0.5 nm, intermediate to heme b_L) is broad and the least stable among the three minima. It is characterized by a water bridge between Q_{O_1} and Y147$_{OH}$, but the interaction of Q with H152 is either a direct H-bond (Figure 5D) or a water bridge (Figure 5E). These two binding modes are reactive configurations that could readily transfer phenolic protons during Q oxidation, suggesting that Y147 in cyt *b* and H152 in the Rieske protein are the initial acceptors of protons released.

The third binding mode (at 0.85 nm, "distal" to heme b_L) is characterized by a weak interaction between Q_{O_4} and H152$_{N_\epsilon}$ and a lack of contact between Q_{O_1} and Y147$_{OH}$ (Figure 5F), disabling proton transfer between these groups. This minimum is separated from the previous two minima by a ~10−15 kJ/mol barrier, making this third mode relatively stable.

Remarkably, this distal mode corresponds to the Q binding mode found among all experimental bc_1 structures deposited in the PDB in which a Q substrate binds to the Q_o site.[13−19] These PDB structures, obtained recently from various organisms and with substrates of variable Q-tail length, show distances of H152$_{N_\epsilon}$···Q_{O_4} between 0.3 and 0.5 nm and Y147$_{OH}$···Q_{O_1} between 0.8 and 1.0 nm, in line with the mode in Figure 5F. Thus, we suggest that the distal mode represents a stable prereactive conformation that could be observed in typical cryo-EM experiments,[13−16] while the other two more proximal modes (Figure 5) are in dynamic exchange and cannot be captured by cryo-EM due to the high flexibility and proposed reactivity (short lifetime during the Q-cycle) of the Q substrate.

The three binding modes are observed for both −*g* and *t* conformers of the Y147 side chain, while its *g* form often leads to slight dissociation of the Q-head from the Q_o site, disrupting the contact between Q_{O_4} and H152. The configuration with a double H-bond found in the distance pair (0.3,0.3) nm shown in Figure 5C has low stability and was not considered a stable binding mode. It was observed in simulations only when Y147 was in the *t* form. Thus, Y147 flexibility modulates the binding interactions of the Q-head and its contacts with H152.

The minimum in the profile centered at pair (0.6,1.0) nm corresponds to the Q-head bent toward heme b_L, observed only in a stretch of one metadynamics trajectory (mentioned above). This region does not represent a Q binding mode and may be an intermediate for the substrate binding pathway, such as proposed for Q binding in other respiratory enzymes.[63,64]

The stability of other direct contacts involving YEY side chains was evaluated in Figure 6, with free energy profiles

https://doi.org/10.1021/acs.jcim.5c00655
J. Chem. Inf. Model. 2025, 65, 6184−6197

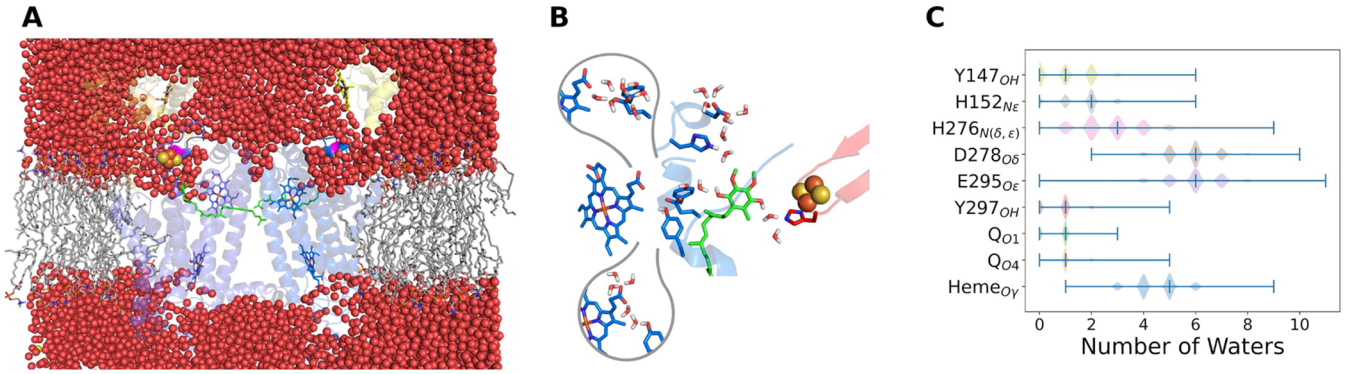

Figure 7. Hydration of the cytochrome bc_1 dimer complex. (A) Global solvation of the protein model embedded in the membrane with lipids in gray sticks, in the same orientation and color code of Figure 1A. Water molecules (oxygen in red spheres) penetrate and solvate the Q_o site, with direct contact from bulk water to heme PRA$_{b_L}$ (blue sticks) and to D278 (magenta). (B) Close view of the Q_o site with average number of bound water molecules found in simulations, in the same orientation of Figure 1B. The two bubble insets focus on hydration of PRA$_{b_L}$ and YEY residues which were removed from the main panel for clarity. (C) Distribution of the number of water molecules under H-bond distance to centers in the Q_o site listed in the *Y*-axis as obtained from the MD simulations. Minimum, median and maximum numbers for each center are shown as ticks.

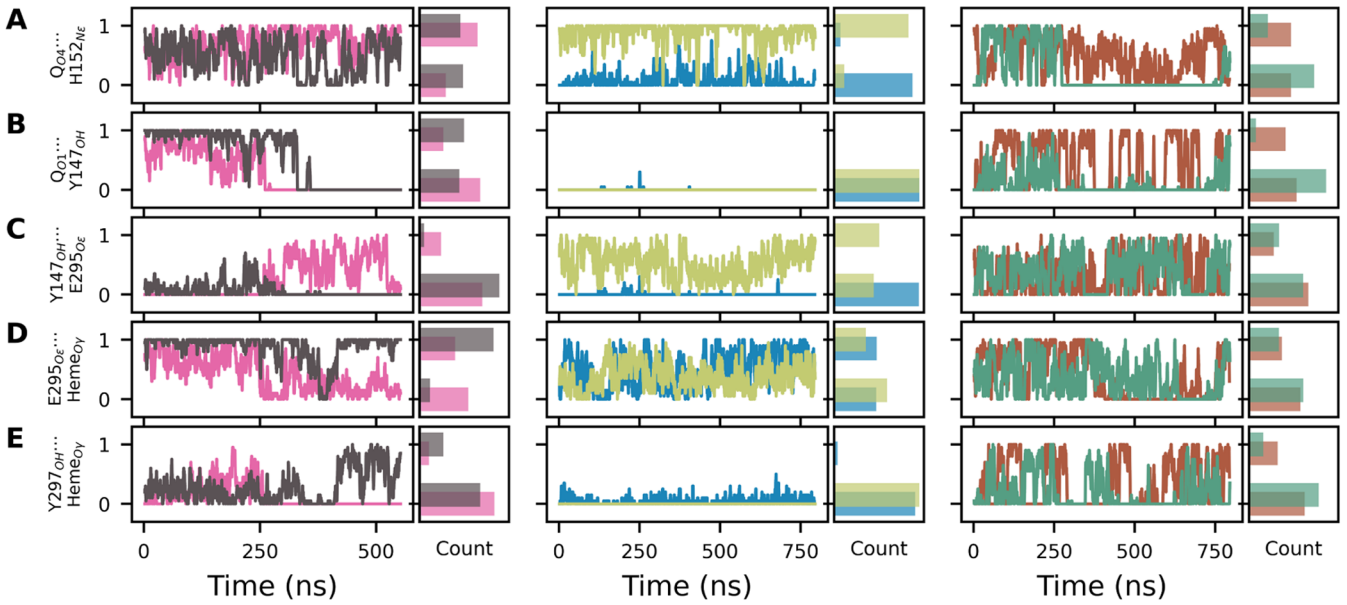

Figure 8. Contacts bridged by one water molecule during simulations. Panel columns and colors relate to the six MD simulations of the Q_o site as described in Figure 4. Contacts are given in *Y*-axis labels and a bridge water is denoted by dots (···). One or zero correspond to the contact formed or not, respectively. A moving-average with a 1 ns window is plotted. Count shows a histogram of contact formation.

estimated from the metadynamics simulations. The interaction between the O_1 phenolic oxygen in Q and the E295 side chain (C_δ is used as a reference since both O_ϵ can form H-bonds) is weak (minimum <5 kJ/mol) and these groups are more stable when separated by ∼0.7 nm (Figure 6A). Side-chains of Y147 and E295 are highly flexible (Figure 3), but their inter-residue contact is stable (minimum at 0.5 nm in Figure 6B).

The Y147 and Y297 side chains can also H-bond (minimum at 0.3 nm in Figure 6C), but it is difficult to quantify their stability because this free energy profile has a large variance and is less reliable at longer pair distances. This H-bond is only formed when Y147 and Y297 residues are in the $(-g, g)$ conformer (Figure 3H). Heme b_L A-propionate (PRA$_{b_L}$) does not (or very rarely) form direct H-bonds with side chains of the YEY group (Figure S4A−C). However, PRA$_{b_L}$ can interact with the YEY residues via multiple water bridges, as depicted in the next section.

The role of H276 in proton transfer from the Q substrate[30] can be evaluated from its contacts in the Q_o site. H276 does not interact directly or via a water bridge with either the substrate Q-head (Figures S4D and S5F) or residue Y147 (Figures 6D and S5G). However, H276 and E295 form a weak inter-residue contact (minimum <5 kJ/mol, Figure 6E). Thus, H276 should not receive a proton directly from the Q-head or from the proposed initial acceptor Y147, and may participate in the proton transfer pathway only if receiving it from E295. The connection between H276 and D278, another proposed proton release group,[30] can be easily established directly (Figure S4E) or via water bridges (Figure S5C,D).

Q_o Site is Highly Hydrated and Has Several Water-Bridged Connections between Side Chains. Figure 7A shows a snapshot of the complete and equilibrated bc_1 model used in our MD simulations, with the solvated and membrane-embedded protein. It is evident that water can penetrate the Q_o site and connect the bulk to PRA$_{b_L}$ and to D278. This allows

https://doi.org/10.1021/acs.jcim.5c00655
J. Chem. Inf. Model. 2025, 65, 6184−6197

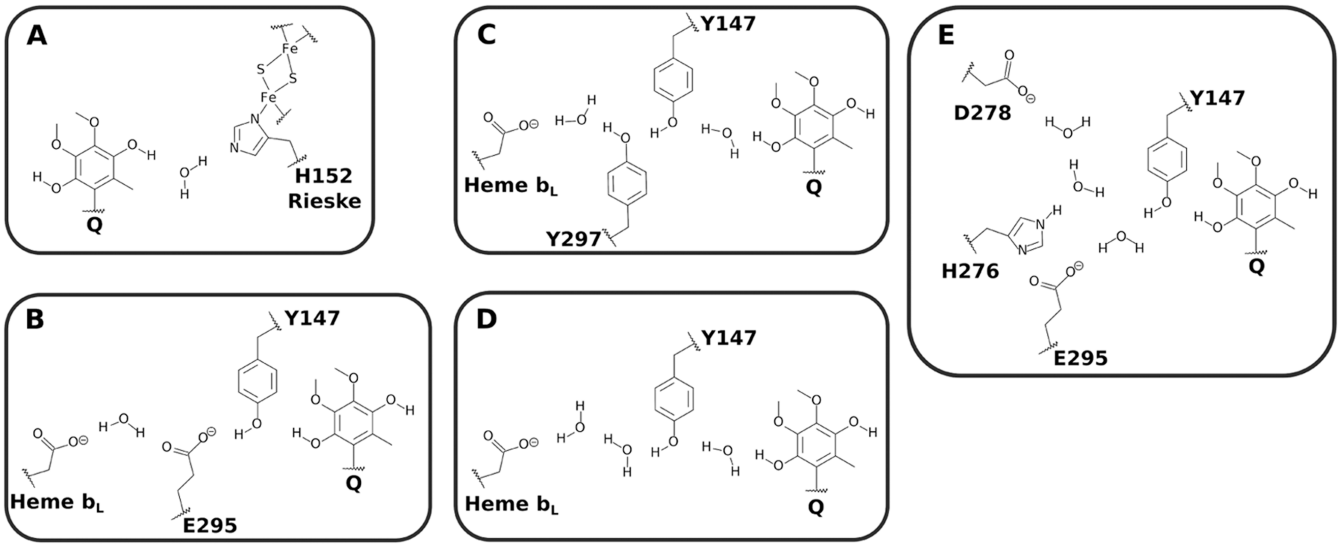

Figure 9. Proton-wires proposed to transfer the two chemical H^+ generated by oxidation of the quinol substrate to proton release groups. (A) Pathway for proton transfer from Q_{O_4} to H152 in the Rieske protein. (B−D) Pathways from Q_{O_1} to heme PRA_{b_L}. (E) Pathway from Q_{O_1} to D278 in cyt *b*.

water to transit quickly and ensures high hydration within the Q_o site.

Figure 7B illustrates the average local hydration in MD simulations, as quantified in Figure 7C. For instance, acidic oxygens in E295, D278, and heme PRA_{b_L} are highly hydrated, with a median of 5 to 6 water molecules each. The extensive solvation of D278 and PRA_{b_L}, which are in contact with external water, suggests that these groups may function as proton release groups, i.e., as the last protein acceptors of the chemical proton before it is transferred to bulk water.

Polar oxygens in residues Y147, Y297, and in the quinol substrate (O_1 and O_4) are hydrated by only one molecule each on average (Figure 7B,C). However, significantly higher water H-bond lifetimes (t_{life}, calculated from the canonical MD simulations) reaching 4 ns for Q_{O_1} and 0.4−0.3 ns for the other three groups are observed for these groups.

For the H-bond between Q_{O_1} and water, t_{life} is 3 orders of magnitude longer than simulated with the same energy model for a free and unbound quinol molecule embedded in lipid-only bilayers.[38,39] On the other hand, t_{life} for water H-bonded to D278 and PRA_{b_L}, which have higher hydration and are in direct contact with the bulk, are 0.1 ns or lower and similar to bulk water t_{life}. This suggests that the Q_o site stabilizes local hydration to facilitate the formation of proton-conducting wires, with water diffusion increasing with distance from the initial proton donor (Q substrate here).

Several contacts between the substrate, binding residues and heme b_L in this highly hydrated Q_o site are mediated by water molecules in bridge. These contacts are essential to establish proton-wires that may be used in a Grotthuss mechanism of proton transfer.

Figures 8 and S5 show trajectories during MD simulations for contacts that may mediate proton transfer from the Q substrate to heme and to D278. Due to their boosted potential, metadynamics simulations (last panel column in Figures 8 and S5) show more frequent contact exchange and a more even histogram between simulations of the two Q_o sites in the bc_1 dimer, while canonical MDs (first and second panel columns in these Figures) have less exchange and more dispersion, with the dynamics of contacts depending more on their (different) initial configuration.

Bridges are frequently and briefly disrupted when the bridged water exchanges with another water molecule (fast oscillations in Figure 8), but bridges are disrupted persistently when their respective donor−acceptor centers move away. For instance, the bridge $Q_{O_4}\cdots H152_{N_\epsilon}$ is disrupted at ∼250 ns in the green trajectory of Figure 8A, corresponding to the increase in distance between these centers in the same trajectory shown in Figure 4B.

A similar observation can be made for the bridge $Q_{O_1}\cdots Y147_{OH}$ (compare Figure 8B to 4C). Here, three characteristic distances are observed (in agreement with the minima found in the free energy profile of Figure 5A), and the water-mediated bridge can only be established when the distance between Q_{O_1} and $Y147_{OH}$ is ∼0.5 nm. Bridged contacts involving phenolic oxygens (O_1 and O_4) in Q are the most persistent, with an average lifetime of 0.4 ns, while other bridge contacts involving putative proton acceptors remain for less than 0.2 ns.

Bridged contacts between Y147 and E295, and between heme PRA_{b_L} and E295 or Y297, can often be formed (Figure 8C−E), suggesting a combination of possible proton-wires to deliver a chemical H^+ to heme. Interestingly, a direct (Figure 6A) or a bridged water contact between E295 and the Q-head are not (or very rarely) established, and E295 should only participate in proton-wires that transfer a chemical H^+ from the Q substrate via Y147 (Figure S5E). Additional bridged contacts of heme b_L with $Y147_{OH}$ via two sequential waters, and with Q_{O1} via three sequential bridged waters, may also be established (Figure S5A,B). $H276_{N_{(\epsilon,\delta)}}$ can also connect to $D278_{O_\delta}$ via bridges with one or two water molecules (Figure S5C,D).

Thus, a dynamic network of H-bonds is established in the Q_o site, as all bridged contacts shown in Figure 8 remain formed during a non-negligible fraction of the simulated time. For instance, the least stable bridge in this figure, $Y297_{OH}\cdots Heme_{O_7}$, is established 16% of the simulation time.

It should be noted that previous MD simulations suggested a mostly dry Q_o site that lacked an H-bond network mediated by water molecules[23,25] in disagreement with the present results and with recent cryo-EM structures (Figure 11). Another MD

https://doi.org/10.1021/acs.jcim.5c00655
J. Chem. Inf. Model. 2025, 65, 6184−6197

simulation included the participation of water in the Q_o site but dismissed a role for Y147 and emphasized E295 as an initial proton acceptor.[22] We attribute these differences compared to the present results to two important methodological improvements in our study. The force-field used to describe the Q substrate in previous simulations[22,23,25] has been shown to contain errors in torsional potentials and electric dipoles[38] and led to inaccurate partition free energies compared to experiments,[39] possibly due to exaggerated hydrophobicity of the Q-head.

Here, we employed a force-field calibrated for Q interactions, which has been shown to provide superior performance[38,39] and thus, has become the *de facto* standard to simulate Q molecular dynamics.[64−66] We also performed simulations 1 order of magnitude longer (in aggregated time) and had conformational sampling enhanced by metadynamics, allowing significantly more sampling of flexible side chains and important interactions in the Q_o site.

Multiple Proton-Wires are Identified and Connect the Q Substrate to Various Proton Acceptors. By combining this hydration analysis with the direct contacts and side chain flexibility described in the previous section (Figures 3 and 6), we suggest multiple proton-wires to transfer the two chemical H^+ released after quinol oxidation in the Q_o site (Figure 9). Three different wires connect Q_{O_1} to heme PRA_{b_L}, one wire connects Q_{O_1} to D278, and one wire from Q_{O_4} to H152. Y147 is the initial acceptor from Q_{O_1} in all proposed proton-wires, and H152 is the initial (and only) acceptor from Q_{O_4}.

Contacts between heme PRA_{b_L} and residues of the YEY group can only be established via water bridges. On the other hand, contacts between Q_{O_4} and H152, Q_{O_1} and Y147, Y147 and E295, and between H276 and D278 may be established directly or via water bridges (Figures 5 and 9). It should be noted that the high intrinsic pK_a of Tyr residues makes them effective proton acceptors, and often involves highly concerted transfer mechanisms.[67]

The interplay of direct H-bonds and contacts mediated by water molecules in bridges (H-bonded in series) are established due to the dynamic network of H-bonds in the Q_o site. We refrained from proposing wires with connections containing more than two water molecules in bridge. It is expected that the stability of long wires will decrease with an increasing number of mobile participants, such as bridge waters, due to the entropic penalty of having all groups aligned simultaneously.[32,68] Yet, the presence of multiple wires may reduce this entropic penalty and avoid disruption of function in point mutants of participating residues.

In a follow-up study recently published,[69] we employed hybrid QM/MM potentials[37,70,71] to simulate proton transfer reactions along the proton wires identified in this work. Multiple oxidation states of reactants at the Q_o site were investigated, including the putative semiquinone state. The results elucidated the energetics of proton transfer, detailing the mechanisms of bond-breaking and bond-forming sequences, as well as the protonation states and composition of participating groups.

Efficient proton conduction was observed for wires A, B, C, and D in Figure 9, confirming that H152 and Y147 act as proton acceptors from Q_{O_4} and Q_{O_1}, respectively. Proton transfers from Q_{O_1} via Y147 (through pathways B, C, and D) to PRA_{b_L} exhibited barriers of 25−40 kJ/mol and reaction free energies of ±10 kJ/mol, indicating that these pathways are thermodynamically feasible and kinetically fast.[69] These findings support the viability of heme PRA_{b_L} as an acceptor for the second proton, as proposed here. Transfers occur via a highly concerted Grotthuss-like mechanism, involving E295, Y297, and bound water molecules in the Q_o site, as identified here (Figures 7 and 11).

Thus, pathways B, C, and D operate redundantly, forming a robust proton-conducting network. The protonation states of the YEY side chains before and after proton transfer remained consistent with those modeled here, with no tyrosinate anion formation observed in either Y147 or Y297.[69]

Site-directed mutagenesis at the Q_o site has been widely studied in experiments aimed at determining residues involved in proton transport.[4,72] However, their interpretation must consider that point mutations may perturb local conformations (or even global protein stability and assembly) and lead to the indirect deactivation of proton transfer pathways without necessarily knocking out a residue that chemically reacts. Also, proton transfer is often fast, may not be rate-limiting, and may operate through various proton-wires. Thus, multiple mutations may have to be combined to significantly slow or alter measured kinetics and organism growth properties.[30] These multiple mutations may also exacerbate the indirect perturbation effect.

Yet, we should mention a few mutational studies in line with the discussion presented here. Exchange of E295 affects overall bc_1 catalytic activity but does not completely abolish it.[29,73−75] Mutation of Y147 is more drastic, and the bc_1 activity is severely affected, in some cases making electron transfer from quinol to heme b_L impossible.[28,72,76]

One of the open questions about the mechanism of Q oxidation in the Q_o site is the relevance of a semiquinone (radical) intermediary for the bifurcated electron transfer. Although this radical has been experimentally reported,[22,77] the evidence has been debated, particularly in the context of wild-type bc_1 under normal operation of the Q-cycle.[4] The present results show that pathways for proton transfer from Q_{O_4} and Q_{O_1} reform on the ns time scale due to side chain torsions, Q-head flexibility, and local hydration in the Q_o site. We suggest this time scale is a lower bound to the lifetime of the semiquinone intermediary. Two-electron oxidation of the quinol substrate without proton transfer (or generation of a QH_2^{2+} transient species) is highly unlikely, so at least one concerted proton transfer[26] should take place during the oxidation process, requiring the formation of a proton-wire on the ns time scale.

Further details on the proton transfer reactions catalyzed in the Q_o site along the proton wires proposed here, including thermodynamic and kinetic analysis of the reaction and the stability of the semiquinone intermediate, can be found in the follow-up study recently published.[69]

Experimental Structures Confirm That Q_o Side Chains are Flexible and Highly Hydrated. We collected 79 experimental structures of the Q_o site previously deposited in the PDB to analyze the distribution of side chain conformers and local hydration (see details in "Analysis of Experimental Structures" in Methods and "Details of bc1 Experimental Structures Analyzed Here" and Table S1 in the SI). Table 1 and Figure 10 show the five principal torsional modes of YEY side chains found experimentally. The most frequent modes (A and B) have Y147, E295, and Y297 $\chi 1$ in the $(t, -g, g)$ conformer and differ only in the E295 $\chi 2$ torsion, with this side chain pointing toward the Q substrate (B) or in the opposite direction (A).

https://doi.org/10.1021/acs.jcim.5c00655
J. Chem. Inf. Model. 2025, 65, 6184−6197

Table 1. Experimental Torsional Modes for YEY Residues Shown in Figure 10 and Found in *N* Structures of the Experimental Set

	Y147	E295		Y297	
mode	$\chi 1$	$\chi 1$	$\chi 2$	$\chi 1$	*N*
A	*t*	−*g*	−*g*	*g*	51
B	*t*	−*g*	*g*	*g*	24
C	*g*	−*g*	−*g*	*g*	2
D	−*g*	−*g*	*g*	*g*	1
E	*t*	*t*	*g*	−*g*	1

Other conformers are observed for YEY side chains, particularly for Y147, which may assume all three conformers, in agreement with our simulation results on the flexibility of these side chains.

It is remarkable that the relative population among binding modes found experimentally is in line with the relative free energies estimated from simulations. For instance, the minima found in the 2D free energy profile for combined Y147 and Y297 torsion (Figure 3D) directly correspond with experimental modes (Table 1) and conformers shown in Figure 3G,H,I map respectively to modes (A,B), D, and E in Figure 10. Relative conformer populations of 1−2%, observed for modes C−E (Table 1), correspond to differences in free energy of ∼10 kJ/mol between their relative stability, as estimated here (Figure 3D). The torsion profile for $\chi 1$ in E295 (Figure 3F) shows the *g* conformer is ∼20 kJ/mol less stable, and this form is not observed in the experimental set.

Given the high variability in the residues found at cyt *b* positions 276 and 278 (Figure 2), H276 and D278 are both present in only half (40) of the 79 experimental Q_o site structures analyzed. D278 $\chi 1$ assumes conformer −*g* in 35 structures. H276 $\chi 1$ is more flexible and assumes either −*g* (19 structures) or *t* (21 structures) forms. In the H276 −*g* torsion, the distance between $H276_{N_{(\delta\epsilon)}}$ and $D276_{C_\gamma}$ is higher than 0.7 nm, and this conformer should be less relevant for the proposed proton-wire (Figure 9E). The distance is reduced to 0.5 nm in the *g* H276 conformer, shown in simulations to be energetically stable (Figure 3E).

Among the experimental structures with resolved water in the Q_o site, up to 5 water molecules were found within a 0.5 nm radius of heme PRA_{b_L}, 4 near Y147, and 3 near Y297, indicating hydration in the Q_o site region and the possibility of water-mediated contacts and proton transfers.

Water-bridged contacts are revealed in various structures. For instance, an X-ray structure bound to stigmatellin (Figure 11A) shows water molecules between heme b_L, Y297, and E295. A recent structure of the supercomplex I + III_2 of *Arabidopsis thaliana* in high resolution shows extensive hydration of the Q_o site[16] (Figure 11B), and reveals a pocket of water molecules near PRA_{b_L}, drawing attention to the role of Y297 and nearby water molecules in mediating proton transfer.

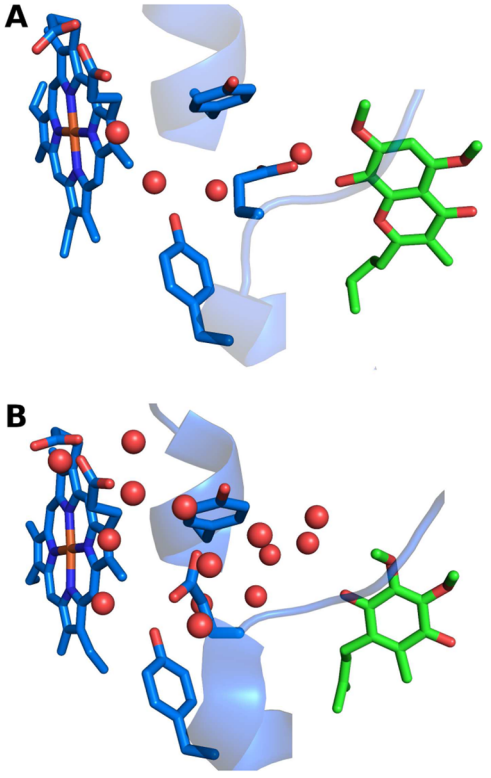

Figure 11. Water molecules observed in experimental structures match hydration contacts simulated for the Q_o site. (A) PDB 1sqx[78] with water between Y297 and heme PRA_{b_L} and between the bound stigmatellin inhibitor and E295. (B) PDB 8bel[16] also with water between Y147, E295 and distal bound Q-head substrate, in line with simulations (Figure 7).

CONCLUSIONS

Molecular dynamics simulations of cytochrome bc_1 provide insights into the conformational landscape of the Q_o site and its binding to the Q substrate in quinol form. Conserved side chains (YEY group of Y147, E295, and Y297) populate multiple conformers, resulting in three binding modes for the Q-head. The two modes proximal to heme b_L may transfer protons upon Q oxidation via direct and water-bridged interactions between Q_{O1} and Y147, and between Q_{O4} and H152, suggesting these

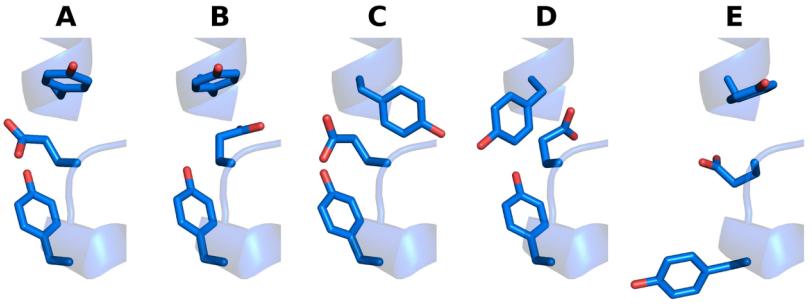

Figure 10. Experimental conformations for Y147, E295 and Y297 (YEY) residues in the Q_o site found among 79 structures of the Q_o site deposited in the PDB. Modes are labeled (A−E) accordingly to Table 1.

https://doi.org/10.1021/acs.jcim.5c00655
J. Chem. Inf. Model. 2025, 65, 6184−6197

residues are initial proton acceptors. The distal binding mode is characterized by a lack of contact between Q_{O_1} and Y147, and is in line with the Q binding mode observed in experimental structures, likely representing a stable prereactive state that is more readily captured in cryo-EM studies.

Analysis of a collection of experimental structures confirms the flexibility of YEY group, particularly for the Y147 and Y297 side chains. This flexibility has not received much attention before. Simulations also indicate that H276 and E295 form weak interactions within the Q_o site and are not initial proton acceptors. Instead, H276 may only engage in indirect proton transfer from Q through Y147 and E295.

MD simulations also reveal that the Q_o site is highly hydrated, with a network of both direct and water-mediated contacts. Key residues such as Y147 and H152 also interact with the Q substrate through these water-bridged connections. PRA_{b_L} only interact with YEY residues via bridged contacts. Thus, multiple proton-conducting wires are established for efficient transfer of protons in a Grotthuss mechanism, highlighting the critical role of hydration in the Q_o site function. This is again supported by experimental structures, particularly recent cryo-EM studies.

Our results agree with the proposed roles for H152 in the Rieske protein for Q binding in the Q_o site and transport of one of the chemical protons released from Q oxidation.[2,4,20] From H152, the excess proton could be passed to bulk water during the characterized movement of the Rieske protein, that approximates the FeS cluster and heme c_1 to continue the electron transfer chain.[4]

An important contribution of this study concerns the groups and proton-wire involved in transport of the secondary proton from Q oxidation. Our results strongly support Y147 as the initial proton acceptor from Q_{O_4}, and we propose for the first time that heme b_L propionate-A is the final protein acceptor before the excess proton is released to the bulk water. An alternative proposal[30] suggesting a proton-wire composed of H276 and D278 seems less likely due to lack of their conservation and the complex, extended pathway (Figure 9E) required.

Multiple proton-wires and a network of H-bonds have been proposed to transport protons in other proteins[79,80] including respiratory complex IV (CcO) which also show proton-wires composed by propionate groups from a redox-active heme.[34−36] Thus, it is not really surprising that cytochrome bc_1 employs similar components and interactions for the molecular mechanism of the Q-cycle in the Q_o site as suggested here by MD simulations. The correlation between our detailed results and experimental data strengthens our understanding of the molecular mechanisms governing proton transfer in cytochrome bc_1, integrating structural flexibility with functional hydration.

In closing, it is notable that other enzymes involved in Q redox reactions appear to use similar residues and strategies for transferring chemical protons to the substrate Q. Respiratory complex I (NADH:ubiquinone oxidoreductase)[63,64] and complex II (succinate dehydrogenase)[81] also contain His and Tyr side chains that hydrogen bond to Q molecules, either directly or via water bridges, within their active sites where Q redox reactions occur. This similarity warrants further investigation to elucidate a general enzymatic mechanism for Q redox chemistry.

■ ASSOCIATED CONTENT

Data Availability Statement

Initial configurations and topology files for all MD simulations were deposited online[82] to enable full reproduction of this study. The GROMACS and PLUMED programs used here are freely available online.

Supporting Information

The Supporting Information is available free of charge at https://pubs.acs.org/doi/10.1021/acs.jcim.5c00655.

Details of bc_1 experimental structures analyzed here, additional force-field parameters for heme *b* and FeS His ligands, accuracy of the MM potential, root-mean-square deviations (RMSD) and fluctuations (RMSF) from MD simulations, convergence of metadynamics simulations and free energy profiles, trajectories of contacts by heme PRA_{b_L} and by H276, and by additional contacts bridged by water, and supporting table for experimental structures analyzed (PDF)

■ AUTHOR INFORMATION

Corresponding Author

Guilherme M. Arantes − *Department of Biochemistry, Instituto de Química, Universidade de São Paulo, 05508-900 São Paulo, SP, Brazil;* orcid.org/0000-0001-5356-7703; Email: garantes@iq.usp.br

Author

Sofia R. G. Camilo − *Department of Biochemistry, Instituto de Química, Universidade de São Paulo, 05508-900 São Paulo, SP, Brazil*

Complete contact information is available at: https://pubs.acs.org/10.1021/acs.jcim.5c00655

Author Contributions

S.R.G.C. performed simulations and analyses. G.M.A. designed the study, performed simulations and analyses, acquired funding, and wrote the manuscript.

Funding

The Article Processing Charge for the publication of this research was funded by the Coordenacao de Aperfeicoamento de Pessoal de Nivel Superior (CAPES), Brazil (ROR identifier: 00x0ma614).

Notes

The authors declare no competing financial interest.

■ ACKNOWLEDGMENTS

Funding from Fundação de Amparo à Pesquisa do Estado de São Paulo (FAPESP, scholarship 2019/05531-0 to S.R.G.C. and grants 2019/21856-7 and 2023/00934-5 to G.M.A.) and computational resources from the SDumont cluster in the LNCC (MCTI) are gratefully acknowledged.

■ REFERENCES

(1) Mitchell, P. The Protonmotive Q-cycle: A General Formulation. *FEBS Lett.* **1975**, *59*, 137−139.

(2) Cramer, W. A.; Hasan, S. S.; Yamashita, E. The Q Cycle of Cytochrome bc Complexes: A Structure Perspective. *Biochim. Biophys. Acta, Bioenerg.* **2011**, *1807*, 788−802.

(3) Xia, D.; Esser, L.; Tang, W.-K.; Zhou, F.; Zhou, Y.; Yu, L.; Yu, C.-A. Structural analysis of cytochrome bc_1 complexes: implications to the mechanism of function. *Biochim. Biophys. Acta, Bioenerg.* **2013**, *1827*, 1278−1294.

(4) Sarewicz, M.; Pintscher, S.; Pietras, R.; Borek, A.; Bujnowicz, Ł.; Hanke, G.; Cramer, W. A.; Finazzi, G.; Osyczka, A. Catalytic Reactions and Energy Conservation in the Cytochrome bc_1 and b_6f Complexes of Energy-Transducing Membranes. *Chem. Rev.* **2021**, *121*, 2020−2108.
(5) Guzy, R. D.; Hoyos, B.; Robin, E.; Chen, H.; Liu, L.; Mansfield, K. D.; Simon, M. C.; Hammerling, U.; Schumacker, P. T. Mitochondrial complex III is required for hypoxia-induced ROS production and cellular oxygen sensing. *Cell Metab.* **2005**, *1*, 401−408.
(6) Murphy, M. P.; Holmgren, A.; Larsson, N.-G.; Halliwell, B.; Chang, C. J.; Kalyanaraman, B.; Rhee, S. G.; Thornalley, P. J.; Partridge, L.; Gems, D.; et al. Unraveling the biological roles of reactive oxygen species. *Cell Metab.* **2011**, *13*, 361−366.
(7) Nixon, G. L.; Moss, D. M.; Shone, A. E.; Lalloo, D. G.; Fisher, N.; O'Neill, P. M.; Ward, S. A.; Biagini, G. A. Antimalarial pharmacology and therapeutics of atovaquone. *J. Antimicrob. Chemother.* **2013**, *68*, 977−985.
(8) Gisi, U.; Sierotzki, H.; Cook, A.; McCaffery, A. Mechanisms influencing the evolution of resistance to Qo inhibitor fungicides. *Pest Manage. Sci.* **2002**, *58*, 859−867.
(9) Esser, L.; Elberry, M.; Zhou, F.; Yu, C.-A.; Yu, L.; Xia, D. Inhibitor-Complexed Structures of the Cytochrome bc_1 from the Photosynthetic Bacterium Rhodobacter sphaeroides. *J. Biol. Chem.* **2008**, *283*, 2846−2857.
(10) Berry, E. A.; Guergova-Kuras, M.; Huang, L.-s.; Crofts, A. R. Structure and function of cytochrome *bc* complexes. *Annu. Rev. Biochem.* **2000**, *69*, 1005−1075.
(11) Crofts, A. R.; Hong, S.; Wilson, C.; Burton, R.; Victoria, D.; Harrison, C.; Schulten, K. The mechanism of ubihydroquinone oxidation at the Q_o-site of the cytochrome bc_1 complex. *Biochim. Biophys. Acta, Bioenerg.* **2013**, *1827*, 1362−1377.
(12) Yuly, J. L.; Zhang, P.; Lubner, C. E.; Peters, J. W.; Beratan, D. N. Universal Free-Energy Landscape Produces Efficient and Reversible Electron Bifurcation. *Proc. Natl. Acad. Sci. U.S.A.* **2020**, *117*, 21045−21051.
(13) Letts, J. A.; Fiedorczuk, K.; Degliesposti, G.; Skehel, M.; Sazanov, L. A. Structures of Respiratory Supercomplex I+III2 Reveal Functional and Conformational Crosstalk. *Mol. Cell* **2019**, *75*, 1131−1146.
(14) Di Trani, J. M.; Liu, Z.; Whitesell, L.; Brzezinski, P.; Cowen, L. E.; Rubinstein, J. L. Rieske head domain dynamics and indazole-derivative inhibition of Candida albicans complex III. *Structure* **2022**, *30*, 129−138.e4.
(15) Swainsbury, D. J. K.; Hawkings, F. R.; Martin, E. C.; Musiał, S.; Salisbury, J. H.; Jackson, P. J.; Farmer, D. A.; Johnson, M. P.; Siebert, C. A.; Hitchcock, A.; Hunter, C. N. Cryo-EM structure of the four-subunit *Rhodobacter sphaeroides* cytochrome bc_1 complex in styrene maleic acid nanodiscs. *Proc. Natl. Acad. Sci. U.S.A.* **2023**, *120*, No. e2217922120.
(16) Klusch, N.; Dreimann, M.; Senkler, J.; Rugen, N.; Kuhlbrandt, W.; Braun, H.-P. CryoEM structure of the respiratory $I + III_2$ supercomplex from Arabidopsis thaliana at 2Å resolution. *Nat. Plants* **2023**, *9*, 142−156.
(17) Hryc, C. F.; Mallampalli, V. K.; Bovshik, E. I.; Azinas, S.; Fan, G.; Serysheva, I. I.; Sparagna, G. C.; Baker, M. L.; Mileykovskaya, E.; Dowhan, W. Structural insights into cardiolipin replacement by phosphatidylglycerol in a cardiolipin-lacking yeast respiratory supercomplex. *Nat. Commun.* **2023**, *14*, No. 2783.
(18) Di Trani, J. M.; Gheorghita, A. A.; Turner, M.; Brzezinski, P.; Ädelroth, P.; Vahidi, S.; Howell, P. L.; Rubinstein, J. L. Structure of the bc_1−cbb_3 respiratory supercomplex from Pseudomonas aeruginosa. *Proc. Natl. Acad. Sci. U.S.A.* **2023**, *120*, No. e2307093120.
(19) Zheng, W.; Chai, P.; Zhu, J.; Zhang, K. High-resolution in situ structures of mammalian respiratory supercomplexes. *Nature* **2024**, *631*, 232−239.
(20) Crofts, A. R.; Guergova-Kuras, M.; Kuras, R.; Ugulava, N.; Li, J.; Hong, S. Proton-coupled electron transfer at the Qo site: what type of mechanism can account for the high activation barrier? *Biochim. Biophys. Acta, Bioenerg.* **2000**, *1459*, 456−466.
(21) Hsueh, K.-L.; Westler, W. M.; Markley, J. L. NMR Investigations of the Rieske Protein from *Thermus thermophilus* Support a Coupled Proton and Electron Transfer Mechanism. *J. Am. Chem. Soc.* **2010**, *132*, 7908−7918.
(22) Postila, P. A.; Kaszuba, K.; Sarewicz, M.; Osyczka, A.; Vattulainen, I.; Róg, T. Key role of water in proton transfer at the Qo-site of the cytochrome bc_1 complex predicted by atomistic molecular dynamics simulations. *Biochim. Biophys. Acta, Bioenerg.* **2013**, *1827*, 761−768.
(23) Barragan, A. M.; Crofts, A. R.; Schulten, K.; Solov'yov, I. A. Identification of Ubiquinol Binding Motifs at the Q_o-Site of the Cytochrome bc_1 Complex. *J. Phys. Chem. B* **2015**, *119*, 433−447.
(24) Hagras, M. A.; Stuchebrukhov, A. A. Internal Switches Modulating Electron Tunneling Currents in Respiratory Complex III. *Biochim. Biophys. Acta, Bioenerg.* **2016**, *1857*, 749−758.
(25) Barragan, A. M.; Schulten, K.; Solov'yov, I. A. Mechanism of the Primary Charge Transfer Reaction in the Cytochrome bc_1 Complex. *J. Phys. Chem. B* **2016**, *120*, 11369−11380.
(26) Camilo, S. R. G.; Curtolo, F.; Galassi, V. V.; Arantes, G. M. Tunneling and Nonadiabatic Effects on a Proton-Coupled Electron Transfer Model for the Q_o Site in Cytochrome bc_1. *J. Chem. Inf. Model.* **2021**, *61*, 1840−1849.
(27) Barragan, A. M.; Soudackov, A. V.; Luthey-Schulten, Z.; Hammes-Schiffer, S.; Schulten, K.; Solov'yov, I. A. Theoretical Description of the Primary Proton-Coupled Electron Transfer Reaction in the Cytochrome bc_1 Complex. *J. Am. Chem. Soc.* **2021**, *143*, 715−723.
(28) Saribas, A. S.; Ding, H.; Dutton, P. L.; Daldal, F. Tyrosine 147 of cytochrome *b* is required for efficient electron transfer at the ubihydroquinone oxidase site (Q_o) of the cytochrome bc_1 complex. *Biochemistry* **1995**, *34*, 16004−16012.
(29) Victoria, D.; Burton, R.; Crofts, A. R. Role of the PEWY-glutamate in catalysis at the Q_o-site of the Cyt bc_1 complex. *Biochim. Biophys. Acta, Bioenerg.* **2013**, *1827*, 365−386.
(30) Borek, A.; Wójcik-Augustyn, A.; Kuleta, P.; Ekiert, R.; Osyczka, A. Identification of hydrogen bonding network for proton transfer at the quinol oxidation site of Rhodobacter capsulatus cytochrome bc_1. *J. Biol. Chem.* **2023**, *299*, No. 105249.
(31) Kaur, D.; Khaniya, U.; Zhang, Y.; Gunner, M. R. Protein Motifs for Proton Transfers That Build the Transmembrane Proton Gradient. *Front. Chem.* **2021**, *9*, No. 660954.
(32) Silverstein, T. P. The Proton in Biochemistry: Impacts on Bioenergetics, Biophysical Chemistry, and Bioorganic Chemistry. *Front. Mol. Biosci.* **2021**, *8*, No. 764099.
(33) Borshchevskiy, V.; Kovalev, K.; Round, E.; et al. True-atomic-resolution insights into the structure and functional role of linear chains and low-barrier hydrogen bonds in proteins. *Nat. Struct. Mol. Biol.* **2022**, *29*, 440−450.
(34) Egawa, T.; Lee, H. J.; Ji, H.; Gennis, R. B.; Yeh, S.-R.; Rousseau, D. L. Identification of heme propionate vibrational modes in the resonance Raman spectra of cytochrome *c* oxidase. *Anal. Biochem.* **2009**, *394*, 141−143.
(35) Warren, J. J.; Mayer, J. M. Proton-Coupled Electron Transfer Reactions at a Heme-Propionate in an Iron-Protoporphyrin-IX Model Compound. *J. Am. Chem. Soc.* **2011**, *133*, 8544−8551.
(36) Goyal, P.; Yang, S.; Cui, Q. Microscopic basis for kinetic gating in cytochrome *c* oxidase: insights from QM/MM analysis. *Chem. Sci.* **2015**, *6*, 826−841.
(37) Kubař, T.; Elstner, M.; Cui, Q. Hybrid Quantum Mechanical/Molecular Mechanical Methods For Studying Energy Transduction in Biomolecular Machines. *Annu. Rev. Biophys.* **2023**, *52*, 525−551.
(38) Galassi, V. V.; Arantes, G. M. Partition, Orientation and Mobility of Ubiquinones in a Lipid Bilayer. *Biochim. Biophys. Acta, Bioenerg.* **2015**, *1847*, 1345−1573.
(39) Teixeira, M. H.; Arantes, G. M. Effects of Lipid Composition on Membrane Distribution and Permeability of Natural Quinones. *RSC Adv.* **2019**, *9*, 16892−16899.
(40) Barducci, A.; Bussi, G.; Parrinello, M. Well-Tempered Metadynamics: A Smoothly Converging and Tunable Free-Energy Method. *Phys. Rev. Lett.* **2008**, *100*, No. 020603.

https://doi.org/10.1021/acs.jcim.5c00655
J. Chem. Inf. Model. 2025, 65, 6184−6197

(41) Biegert, A.; Mayer, C.; Remmert, M.; Soding, J.; Lupas, A. The MPI Bioinformatics Toolkit for protein sequence analysis. *Nucleic Acids Res.* **2006**, *34*, W335−W339.
(42) Crooks, G. E.; Hon, G.; Chandonia, J.-M.; Brenner, S. E. WebLogo: a sequence logo generator. *Genome Res.* **2004**, *14*, 1188−1190.
(43) Lange, C.; Nett, J. H.; Trumpower, B. L.; Hunte, C. Specific Roles of Protein-Phospholipid Interactions in the Yeast Cytochrome bc_1 Complex Structure. *EMBO J.* **2001**, *20*, 6591−6600.
(44) *The PyMOL Molecular Graphics System*, Version 1.8; Schrödinger, LLC, 2015.
(45) Vriend, G. WHAT IF: a Molecular Modeling and Drug Design Program. *J. Mol. Graphics* **1990**, *8*, 52−56.
(46) Klauda, J. B.; Venable, R. M.; Freites, J. A.; O'Connor, J. W.; Tobias, D. J.; Mondragon-Ramirez, C.; Vorobyov, I.; MacKerell, A. D.; Pastor, R. W. Update of the CHARMM All-Atom Additive Force Field for Lipids: Validation on Six Lipid Types. *J. Phys. Chem. B* **2010**, *114*, 7830−7843.
(47) Huang, J.; MacKerell, A. D., Jr CHARMM36 All-Atom Additive Protein Force Field: Validation Based on Comparison to NMR Data. *J. Comput. Chem.* **2013**, *34*, 2135−2145.
(48) Huang, J.; Rauscher, S.; Nawrocki, G.; Ran, T.; Feig, M.; de Groot, B. L.; Grubmuller, H.; MacKerell, A. D., Jr CHARMM36m: an improved force field for folded and intrinsically disordered proteins. *Nat. Methods* **2017**, *14*, 71−73.
(49) Jorgensen, W. L.; Chandrasekhar, J.; Madura, J. D.; Impey, R. W.; Klein, M. L. Comparison of Simple Potential Functions for Simulating Liquid Water. *J. Chem. Phys.* **1983**, *79*, 926−935.
(50) Chang, C. H.; Kim, K. Density Functional Theory Calculation of Bonding and Charge Parameters for Molecular Dynamics Studies on [FeFe] Hydrogenases. *J. Chem. Theory Comput.* **2009**, *5*, 1137−1145.
(51) Autenrieth, F.; Tajkhorshid, E.; Baudry, J.; Luthey-Schulten, Z. Classical force field parameters for the heme prosthetic group of cytochrome *c*. *J. Comput. Chem.* **2004**, *25*, 1613−1622.
(52) Darden, T.; York, D.; Pedersen, L. Particle mesh Ewald: An N·log(N) method for Ewald sums in large systems. *J. Chem. Phys.* **1993**, *98*, 10089−10092.
(53) Hunter, J. D. Matplotlib: A 2D graphics environment. *Comput. Sci. Eng.* **2007**, *9*, 90−95.
(54) Abraham, M. J.; Murtola, T.; Schulz, R.; Pall, S.; Smith, J. C.; Hess, B.; Lindahl, E. GROMACS: High Performance Molecular Simulations Through Multi-Level Parallelism from Laptops to Supercomputers. *SoftwareX* **2015**, *1−2*, 19−25.
(55) Tribello, G. A.; Bonomi, M.; Branduardi, D.; Camilloni, C.; Bussi, G. Plumed 2: New feathers for an old bird. *Comput. Phys. Commun.* **2014**, *185*, 604−613.
(56) Nunes-Alves, A.; Arantes, G. M. Ligand-receptor affinities computed by an adapted linear interaction model for continuum electrostatics and by protein conformational averaging. *J. Chem. Inf. Model.* **2014**, *54*, 2309−2319.
(57) Bairoch, A.; Apweiler, R. The SWISS-PROT protein sequence database and its supplement TrEMBL in 2000. *Nucleic Acids Res.* **2000**, *28*, 45−48.
(58) Hauska, G.; Nitschke, W.; Herrmann, R. G. Amino Acid Identities in the Three Redox Center-Carrying Polypeptides of Cytochrome bc_1/b_6f Complexes. *J. Bioenerg. Biomembr.* **1988**, *20*, 211−228.
(59) Gao, X.; Wen, X.; Yu, C.; Esser, L.; Tsao, S.; Quinn, B.; Zhang, L.; Yu, L.; Xia, D. The Crystal Structure of Mitochondrial Cytochrome bc_1 in Complex with Famoxadone: The Role of Aromatic-Aromatic Interaction in Inhibition. *Biochemistry* **2002**, *41*, 11692−11702.
(60) Ouchane, S.; Agalidis, I.; Astier, C. Natural resistance to inhibitors of the ubiquinol cytochrome c oxidoreductase of Rubrivivax gelatinosus: sequence and functional analysis of the cytochrome bc(1) complex. *J. Bacteriol.* **2002**, *184*, 3815−3822.
(61) Kao, W.-C.; Hunte, C. The Molecular Evolution of the Qo Motif. *Genome Biol. Evol.* **2014**, *6*, 1894−1910.
(62) Gupta, R. S. The phylogeny of proteobacteria: relationships to other eubacterial phyla and eukaryotes. *FEMS Microbiol. Rev.* **2000**, *24*, 367−402.
(63) Hoias Teixeira, M.; Arantes, G. M. Balanced Internal Hydration Discriminates Substrate Binding to Respiratory Complex I. *Biochim. Biophys. Acta, Bioenerg.* **2019**, *1860*, 541−548.
(64) Chung, I.; Wright, J. J.; Bridges, H. R.; Ivanov, B. S.; Biner, O.; Pereira, C. S.; Arantes, G. M.; Hirst, J. Cryo-EM structures define ubiquinone-10 binding to mitochondrial complex I and conformational transitions accompanying Q-site occupancy. *Nat. Commun.* **2022**, *13*, No. 2758.
(65) Parey, K.; Haapanen, O.; Sharma, V.; Köfeler, H.; Züllig, T.; Prinz, S.; Siegmund, K.; Wittig, I.; Mills, D. J.; Vonck, J.; Kühlbrandt, W.; Zickermann, V. High-resolution cryo-EM structures of respiratory complex I: Mechanism, assembly, and disease. *Sci. Adv.* **2019**, *5*, No. eaax9484.
(66) Fuller, J. T.; Barnes, S.; Sadun, L. A.; Ajmera, P.; Alexandrova, A. N.; Sadun, A. A. Coenzyme Q_{10} trapping in mitochondrial complex I underlies Leber's hereditary optic neuropathy. *Proc. Natl. Acad. Sci. U.S.A.* **2023**, *120*, No. e2304884120.
(67) Zdorevskyi, O.; Djurabekova, A.; Lasham, J.; Sharma, V. Horizontal proton transfer across the antiporter-like subunits in mitochondrial respiratory complex I. *Chem. Sci.* **2023**, *14*, 6309−6318.
(68) Pantazis, D. A. Clues to how water splits during photosynthesis. *Nature* **2023**, *617*, 468−469.
(69) Arantes, G. M. Redox-Activated Proton Transfer through a Redundant Network in the Qo Site of Cytochrome bc1. *J. Chem. Inf. Model.* **2025**, *65*, 2660−2669.
(70) Arantes, G. M. The Catalytic Acid in the Dephosphorylation of the Cdk2-pTpY/CycA Protein Complex by Cdc25B Phosphatase. *J. Phys. Chem. B* **2008**, *112*, 15244−15247.
(71) Teixeira, M. H.; Curtolo, F.; Camilo, S. R. G.; Field, M. J.; Zheng, P.; Li, H.; Arantes, G. M. Modeling the Hydrolysis of Iron-Sulfur Clusters. *J. Chem. Inf. Model.* **2020**, *60*, 653−660.
(72) Brasseur, G.; Saribas, A.; Daldal, F. A compilation of mutations located in the cytochrome *b* subunit of the bacterial and mitochondrial bc_1 complex. *Biochim. Biophys. Acta, Bioenerg.* **1996**, *1275*, 61−69.
(73) Seddiki, N.; Meunier, B.; Lemesle-Meunier, D.; Brasseur, G. Is cytochrome *b* glutamic acid 272 a quinol binding residue in the bc_1 complex of Saccharomyces cerevisiae? *Biochemistry* **2008**, *47*, 2357−2368.
(74) Wenz, T.; Hellwig, P.; MacMillan, F.; Meunier, B.; Hunte, C. Probing the role of E272 in quinol oxidation of mitochondrial complex III. *Biochemistry* **2006**, *45*, 9042−9052.
(75) Osyczka, A.; Zhang, H.; Mathé, C.; Rich, P. R.; Moser, C. C.; Dutton, P. L. Role of the PEWY Glutamate in Hydroquinone-Quinone Oxidation-Reduction Catalysis in the Q_o Site of Cytochrome bc_1. *Biochemistry* **2006**, *45*, 10492−10503.
(76) Wenz, T.; Covian, R.; Hellwig, P.; MacMillan, F.; Meunier, B.; Trumpower, B. L.; Hunte, C. Mutational analysis of cytochrome b at the ubiquinol oxidation site of yeast complex III. *J. Biol. Chem.* **2007**, *282*, 3977−3988.
(77) Vennam, P. R.; Fisher, N.; Krzyaniak, M. D.; Kramer, D. M.; Bowman, M. K. A. Caged, Destabilized, Free Radical Intermediate in the Q-Cycle. *ChemBioChem* **2013**, *14*, 1745−1753.
(78) Esser, L.; Quinn, B.; Li, Y.-F.; Zhang, M.; Elberry, M.; Yu, L.; Yu, C.-A.; Xia, D. Crystallographic Studies of Quinol Oxidation Site Inhibitors: A Modified Classification of Inhibitors for the Cytochrome bc_1 Complex. *J. Mol. Biol.* **2004**, *341*, 281−302.
(79) Gregory, M. T.; Gao, Y.; Cui, Q.; Yang, W. Multiple deprotonation paths of the nucleophile 3′−OH in the DNA synthesis reaction. *Proc. Natl. Acad. Sci. U.S.A.* **2021**, *118*, No. e2103990118.
(80) Cai, X.; Haider, K.; Lu, J.; Radic, S.; Son, C. Y.; Cui, Q.; Gunner, M. Network analysis of a proposed exit pathway for protons to the P-side of cytochrome c oxidase. *Biochim. Biophys. Acta, Bioenerg.* **2018**, *1859*, 997−1005.
(81) Iverson, T. Catalytic mechanisms of complex II enzymes: A structural perspective. *Biochim. Biophys. Acta, Bioenerg.* **2013**, *1827*, 648−657.

https://doi.org/10.1021/acs.jcim.5c00655
J. Chem. Inf. Model. 2025, 65, 6184−6197

(82) Arantes, G. M.; Camilo, S. R. G. Dataset for manuscript: Flexibility and hydration of the Qo site determine multiple pathways for proton transfer in cytochrome bc1. 2025 DOI: 10.5281/zenodo.15084037. Accessed: March 25, 2025.

https://doi.org/10.1021/acs.jcim.5c00655
J. Chem. Inf. Model. 2025, 65, 6184−6197